Acta Crystallographica Section D
Biological Crystallography
ISSN 1399-0047

Structural and functional characterization of an arylamine *N*-acetyltransferase from the pathogen *Mycobacterium abscessus*: differences from other mycobacterial isoforms and implications for selective inhibition

Angélique Cocaign,[a]‡§ Xavier Kubiak,[a]‡¶ Ximing Xu,[a] Guillaume Garnier,[b,c] Inès Li de la Sierra-Gallay,[d] Linh Chi-Bui,[a] Julien Dairou,[a] Florent Busi,[a] Areej Abuhammad,[e,f] Ahmed Haouz,[g] Jean-Marie Dupret,[a] Jean-Louis Herrmann[b,c] and Fernando Rodrigues-Lima[a]*

[a]Université Paris Diderot, Sorbonne Paris Cité, Unité de Biologie Fonctionnelle et Adaptative, CNRS UMR 8251, 75013 Paris, France, [b]EA 3647, Université Versailles St Quentin en Yvelines, Garches, France, [c]Laboratoire de Microbiologie, Assistance Publique – Hôpitaux de Paris, Hôpital Raymond Poincaré, Garches, France, [d]Université Paris-Sud, Institut de Biochimie et Biophysique Moléculaire et Cellulaire, CNRS UMR 8619, 91405 Orsay, France, [e]Department of Pharmacology, University of Oxford, Mansfield Road, Oxford OX1 3QT, England, [f]Faculty of Pharmacy, University of Jordan, Queen Rania Street, Amman 11942, Jordan, and [g]Institut Pasteur, Plateforme 6, CNRS–URA2185, 25 Rue du Dr Roux, 75724 Paris, France

‡ AC and XK contributed equally to this work and should be considered joint first authors.
§ Present address: Laboratoire Universitaire Biodiversité et Écologie Microbienne (LUBEM), Université de Brest, Technopôle Brest-Iroise, 29280 Plouzané, France.
¶ Present address: Molecular Neuropharmacology and Genetics Laboratory, Department of Neuroscience and Pharmacology, University of Copenhagen, DK-2200 Copenhagen, Denmark.

Correspondence e-mail: fernando.rodrigues-lima@univ-paris-diderot.fr

Received 23 June 2014
Accepted 24 September 2014

PDB reference: arylamine *N*-acetyltransferase, 4guz

Mycobacterium abscessus is the most pathogenic rapid-growing mycobacterium and is one of the most resistant organisms to chemotherapeutic agents. However, structural and functional studies of *M. abscessus* proteins that could modify/inactivate antibiotics remain nonexistent. Here, the structural and functional characterization of an arylamine *N*-acetyltransferase (NAT) from *M. abscessus* [(MYCAB)NAT1] are reported. This novel prokaryotic NAT displays significant *N*-acetyltransferase activity towards aromatic substrates, including antibiotics such as isoniazid and *p*-aminosalicylate. The enzyme is endogenously expressed and functional in both the rough and smooth *M. abscessus* morphotypes. The crystal structure of (MYCAB)NAT1 at 1.8 Å resolution reveals that it is more closely related to *Nocardia farcinica* NAT than to mycobacterial isoforms. In particular, structural and physicochemical differences from other mycobacterial NATs were found in the active site. Peculiarities of (MYCAB)NAT1 were further supported by kinetic and docking studies showing that the enzyme was poorly inhibited by the piperidinol inhibitor of mycobacterial NATs. This study describes the first structure of an antibiotic-modifying enzyme from *M. abscessus* and provides bases to better understand the substrate/inhibitor-binding specificities among mycobacterial NATs and to identify/optimize specific inhibitors. These data should also contribute to the understanding of the mechanisms that are responsible for the pathogenicity and extensive chemotherapeutic resistance of *M. abscessus*.

1. Introduction

Rapidly growing mycobacteria (RGM) are usually harmless saprophytes, whereas slowly growing mycobacteria (SGM) such as *Mycobacterium tuberculosis* include most of the human-pathogenic species. *M. abscessus* is one of the few RGM that are able to infect humans and causes a broad spectrum of infections (Brown-Elliott & Wallace, 2002; Griffith *et al.*, 1993). *M. abscessus* is now recognized as the prominent *Mycobacterium*, along with *M. avium*, involved in broncho-pulmonary infections in patients with cystic fibrosis or chronic pulmonary disease (Pierre-Audigier *et al.*, 2005; Jönsson *et al.*, 2007). In addition, *M. abscessus* is one of the most resistant organisms to chemotherapeutic agents (Nessar *et al.*, 2012). It is also resistant to most disinfectants and thrives in the most hostile environments (Brown-Elliott & Wallace, 2002). Such resistance is the result of a complex interplay between natural and acquired mechanisms, including the presence of a waxy impermeable cell wall, drug-export systems and genetic polymorphism of targeted genes

(Lambert, 2002; Nash *et al.*, 2009; Nessar *et al.*, 2012). In addition, *M. abscessus* produces enzymes that potentially degrade or modify antibiotics such as β-lactamases, phosphotransferases or acetyltransferases, which can result in their inactivation (Flores *et al.*, 2005; Ramirez & Tolmasky, 2010).

Arylamine *N*-acetyltransferases (NATs) are intracellular xenobiotic-metabolizing enzymes (XMEs) that are responsible for the acetylation of aromatic amines. In humans, these enzymes are important in the metabolism of drugs and have been shown to acetylate and inactivate several antibacterial compounds, including the front-line anti-tuberculosis drugs isoniazid (INH) and *p*-aminosalicylate (4-AS) (Hein *et al.*, 2000; Sim *et al.*, 2012). Interestingly, NAT enzymes are also expressed in several prokaryotes, where they could contribute to adaptive and/or defence mechanisms towards environmental toxins present in the different habitats of bacteria (Payton, Mushtaq *et al.*, 2001; Kubiak *et al.*, 2012; Sim *et al.*, 2012). In addition, certain bacterial NATs have been shown to acetylate and inactivate different antibiotics (Payton *et al.*, 1999; Pluvinage *et al.*, 2007; Sim, Walters *et al.*, 2008). For instance, *M. tuberculosis* NAT [(MYCMR)NAT1] is able to acetylate INH and increased expression of this enzyme results in increased INH resistance (Payton *et al.*, 1999). Moreover, deletion of the *nat* gene in *M. smegmatis* and *M. bovis* leads to strains that are more sensitive to INH (Payton, Gifford *et al.*, 2001; Bhakta *et al.*, 2004). In addition, the deletion of *nat* in *M. bovis* also affects cell-wall composition and biosynthesis of mycolic acids, thus increasing susceptibility to antibiotics that permeate the cell wall (Bhakta *et al.*, 2004). NAT enzymes are therefore attractive therapeutic targets for the development of anti-mycobacterial compounds (Sim *et al.*, 2012). Recently, chemicals aimed at inhibiting mycobacterial NAT enzymes (including *M. tuberculosis* and *M. marinum* NATs) have been identified (Sim *et al.*, 2012, 2014). A piperidinol compound (3-benzoyl-4-phenyl-1-methylpiperidinol; compound **1**) was identified as a selective irreversible inhibitor of prokaryotic NATs with anti-mycobacterial activity (Westwood *et al.*, 2010). However, despite the *M. tuberculosis* and *M. marinum* NATs sharing 75% amino-acid sequence identity, a sixfold higher concentration ($\sim$8 μM) is required to fully inhibit the *M. tuberculosis* isozyme (Abuhammad *et al.*, 2012). Structural comparison revealed slight amino-acid differences in the active site which affect substrate and inhibitor selectivity (Abuhammad *et al.*, 2013). These studies underlined that although the use of certain mycobacterial NAT enzymes (such as *M. marinum* NAT) as surrogate models is helpful, the structural and functional characterization of the 'true' target NAT enzyme is required for medicinal chemistry and structure–activity relationship studies (Abuhammad *et al.*, 2013).

Here, we report the structural and functional characterization of a NAT enzyme from *M. abscessus*. (MYCAB)NAT1 is the first *M. abscessus* antibiotic-modifying enzyme to be described at the structural level. Our data provide bases to better understand the substrate/inhibitor-binding specificity of this enzyme in order to identify/optimize small-molecule inhibitors for its selective inhibition and subsequent putative clinical applications. More broadly, our study should contribute to the understanding of the molecular mechanisms contributing to the pathogenicity and antibiotic resistance of *M. abscessus*.

2. Materials and methods

2.1. Mycobacterial strains, growth conditions and materials

All aromatic compounds [4-iodoaniline (4-IA), 4-butoxyaniline (4-BOA), 3,4-dichloroaniline (3,4-DCA), isoniazid (INH), hydralazine (HDZ), 2-aminofluorene (2-AF), 4-aminosalicylate (4-AS), 5-aminosalicylate (5-AS), *para*-aminobenzoic acid (pABA), sulfamethazine (SMZ), sulfamethoxazole (SMX), sulfadiazine (SDZ) and sulfapyridine (SP)], acetyl-CoA and 5,5′-dithiobis-(2-nitrobenzoic acid) (DTNB) were obtained from Sigma–Aldrich. Acetyl-2-AF, acetyl-INH and acetyl-4-AS were purchased from Interchim. Rabbit polyclonal antibodies against *M. abscessus* NAT were generated by Proteogenix (France) using SDS–PAGE-purified recombinant (MYCAB)NAT1 as an immunogen. Smooth (S) and rough (R) variants of *M. abscessus* reference strain CIP 104536T (Rottman *et al.*, 2007) were used for this study. These strains were grown aerobically in Luria–Bertani medium supplemented with 0.05% Tween-80 at 37°C in the dark with low shaking.

2.2. Multiple sequence alignments and phylogenetic analysis

Protein sequences were retrieved from the NCBI GenPept database. Multiple sequence alignments were conducted with *ClustalW* (http://npasa-pbil.ibpc.fr) with default settings and alignment outputs were generated with *ESPript* v.2.2 (http://espript.ibcp.fr). For phylogenetic analysis, the (MYCAB)NAT1 amino-acid sequence was aligned with characterized or putative NATs using the *MUSCLE* algorithm implemented in *MEGA*5 (Tamura *et al.*, 2011). The tree was obtained by the neighbour-joining method using the Dayhoff model. A total of 500 bootstrap replications were performed to determine the statistical support for clades.

2.3. Molecular cloning of (MYCAB)NAT1, protein production and purification

The *(MYCAB)NAT1* ORF (open reading frame) was amplified from genomic DNA of *M. abscessus* strain CIP 104536T (a gift from Dr J.-M. Reyrat) by high-fidelity PCR using Phusion High Fidelity DNA polymerase according to the manufacturer's recommendations (New England Biolabs). The primers used for amplification were 5-CATATGTGGAACGGCGATGAGCTTCAG-3 (sense) and 5-CTCGAGCTACTGCTCGGCCAGCCGCTCCAA-3 (reverse). The PCR products were double-digested using *Nde*I and *Xho*I restriction enzymes (New England Biolabs) and were cloned into a pET-28a plasmid to express His_6-tag fusion recombinant proteins. Cloning was checked by DNA sequencing. *E. coli* BL21 cells transformed with the MYCAB(NAT1)-encoding pET-28a plasmid were used to produce and purify 6×His-tagged recombinant protein. The production and purification of recombinant NAT enzymes have been described elsewhere

(Kubiak *et al.*, 2012; Pluvinage *et al.*, 2011). The purified enzymes [reduced with 1 m*M* dithiothreitol (DTT)] were dialysed against PBS and kept at −80°C until use. Protein concentrations were determined using the Bradford assay (Bio-Rad).

2.4. SDS–PAGE and Western blot analysis

Proteins were separated by SDS–PAGE (12.5% gel), transferred to a nitrocellulose membrane for Western blot analysis and stained with Ponceau Red. Briefly, the membrane was blocked with 5%(*w*/*v*) dried skimmed milk in TBS-T [Tris-buffered saline (50 m*M* Tris, 150 m*M* NaCl) containing 0.2% Tween-20] for 1 h and then washed with TBS-T before incubation with rabbit serum raised against (MYCAB)NAT1 (1:5000 dilution). After washing, secondary conjugated antibodies were added (anti-rabbit at 1:150 000 dilution). Staining was developed by incubation with chemiluminescent solution (ECL Western Blotting, GE Healthcare).

2.5. Enzyme assays and determination of kinetic parameters

The kinetic parameters K_m^{app} and k_{cat} for the acetylation of prototypic aromatic amine substrates were obtained by steady-state kinetics using the 5,5′-dithiobis-(2-nitrobenzoic acid) (DTNB) assay as described by Brooke *et al.* (2003). Briefly, purified recombinant enzymes and arylamine substrates at increasing concentrations were mixed in a 96-well ELISA plate and preincubated (37°C, 2 min) in buffer (25 m*M* Tris–HCl pH 7.5). AcCoA was added to start the reaction (400 µ*M* final concentration) and the plate was incubated at 37°C. The total reaction volume was 100 µl. The reaction was quenched at different time points with 25 µl DTNB (5 m*M*) in guanidine hydrochloride buffer (6.4 *M* guanidine–HCl, 0.1 *M* Tris–HCl pH 7.3). A_{405} was measured using an ELISA plate analyser. Controls were carried out in the absence of enzyme or AcCoA. The amount of CoA in the reaction was determined by comparison with a standard curve obtained using TNB^-. Initial velocities (V_i) were determined on the basis of an ε_{DTNB} at 405 nm of 0.0032 µ*M* cm^{-1}. The apparent kinetic parameters K_m^{app} and k_{cat} were obtained by non-linear curve fitting against the Michaelis–Menten equation using *Kaleidagraph* 3.5 (Synergy Software). Steady-state kinetics were performed in triplicate.

2.6. Crystallization, data collection and structure refinement

Crystallization assays were set up with (MYCAB)NAT1 concentrated to 30 mg ml^{-1} using Spin-X UF ultracentrifugation concentrators (10 kDa molecular-weight cutoff, Corning). A set of 672 different commercially available crystallization conditions were screened by the vapour-diffusion method using a Cartesian Technologies workstation (Santarsiero *et al.*, 2002): briefly, 600 nl of a 1:1 mixture of (MYCAB)NAT1 protein solution and crystallization solution were equilibrated against a 150 µl reservoir in a Greiner plate (Greiner Bio-One). A single crystal of (MYCAB)NAT1 of dimensions 0.1 × 0.1 × 0.05 mm grew after two weeks in 15% PEG 6000, 5% glycerol at 18°C. This single crystal obtained in the initial screening was used flash-cooled in liquid nitrogen using a mixture of 50% Paratone-N and 50% paraffin oil as a cryoprotectant for further X-ray diffraction data collection (0.984 Å, 0.5° oscillation per image, MAR225 detector) on beamline X06DA at the Swiss Light Source (SLS) synchrotron (Paul Scherrer Institute, Switzerland). *XDS* was used for data integration (Kabsch, 2010). For structure solution, molecular-replacement phases were obtained with *Phaser* as implemented in the *CCP*4 program suite (Winn *et al.*, 2011), using the (NOCFA)NAT1 structure (PDB entry 3d9w; Martins *et al.*, 2008) as a search model. The protein structure was obtained by iterative manual rebuilding using *Coot* (Emsley *et al.*, 2010) and the model was further refined using *BUSTER* 2.10.0 (Bricogne *et al.*, 2011). Finally, stereochemical quality and final validation of the model were performed using *MolProbity* and *PROCHECK*, respectively (Chen *et al.*, 2010; Laskowski *et al.*, 1993). Refinement statistics are shown in Table 1. The atomic coordinates and structure factors for (MYCAB)NAT1 have been deposited in the Protein Data Bank under accession code 4guz.

Table 1
Statistics of data collection and refinement for (MYCAB)NAT1.

Values in parentheses are for the highest resolution shell.

Data collection	
Beamline	X06DA, SLS
Wavelength (Å)	0.984
Space group	*C*121
Unit-cell parameters (Å, °)	*a* = 78.67, *b* = 78.76, *c* = 175.98, α = 90.0, β = 89.99, γ = 90.0
Resolution (Å)	38.39–1.80 (1.91–1.80)
R_{merge}† (%)	11.4 (80.6)
$\langle I/\sigma(I)\rangle$	16.40 (2.26)
Completeness (%)	99.5 (97.6)
Multiplicity	3.071 (3.050)
No. of reflections	303342 (47770)
No. of unique reflections	98775 (15638)
Wilson *B* factor (Å^2)	24.63
Refinement	
Resolution (Å)	38.39–1.80
R/R_{free} (%)	21.15/24.51
No. of non-H atoms	
Protein	8964
Solvent	265
Ligands	—
B factors (Å^2)	
Protein	27.57
Water molecules	23.32
Ligands	—
R.m.s.d., bond lengths (Å)	0.009
R.m.s.d., bond angles (°)	0.95
Ramachandran plot (%)	
Favoured	89.0
Allowed	10.6
Disallowed	0.4

† $R_{merge} = \sum_{hkl}\sum_i |I_i(hkl) - \langle I(hkl)\rangle| / \sum_{hkl}\sum_i I_i(hkl)$, where $I_i(hkl)$ is the *i*th observation of reflection *hkl*, while $\langle I(hkl)\rangle$ is the mean intensity of reflection *hkl*.

2.7. Molecular docking

The (MYCAB)NAT1 enzyme structure with an acetylated Cys73 (AcCys73) was prepared by *AmberTools* 1.2 (Case *et al.*, 2012). The AMBER 99SB force-field and GAFF were used for the acetylated (MYCAB)NAT1 force-field parameters.

Protein energy minimization was carried out by *NAMD* 2.9 (Phillips *et al.*, 2005) with 5000 steps. All of the ligands were built by *Avogadro* (Hanwell *et al.*, 2012) and optimized with the MMFF94 force-field. Acetylated (MYCAB)NAT1 and the ligands were prepared by *AutoDockTools* 1.5.6 (Morris *et al.*, 2009), including merging nonpolar H atoms and calculating the Gasteiger charge. AcCys73 and substrates were set as flexible. The docking site was set to the (MYCAB)NAT1 catalytic site. Grid maps were generated by *AutoGrid* 4 according to the atom types of the protein and substrates. Each grid map consisted of 50 × 50 × 50 grid points, with each point at a spacing of 0.375 Å. Conformations were searched by *AutoDock* 4 using a Lamarckian genetic algorithm (LGA). Finally, the conformation in the lowest energy cluster was selected for analysis of the correlation between pK_m^{app} ($-\log K_m^{app}$) and predicted binding energy.

2.8. Lysate preparation and determination of endogenous NAT activity

Fresh exponential (OD at 600 nm = 0.8) phase cultures (50 ml) of *M. abscessus* morphotypes S and R were resuspended in 400 µl 25 m*M* Tris–HCl pH 7.5, protease-inhibitor cocktail, 2.5 mg ml^{-1} lysozyme, 0.1% Triton X-100 and sonicated for 30 s (2 s pulse on, 10 s pulse off) at 4°C. Proteins were reduced with 5 m*M* DTT and the concentration was estimated using the Bradford assay.

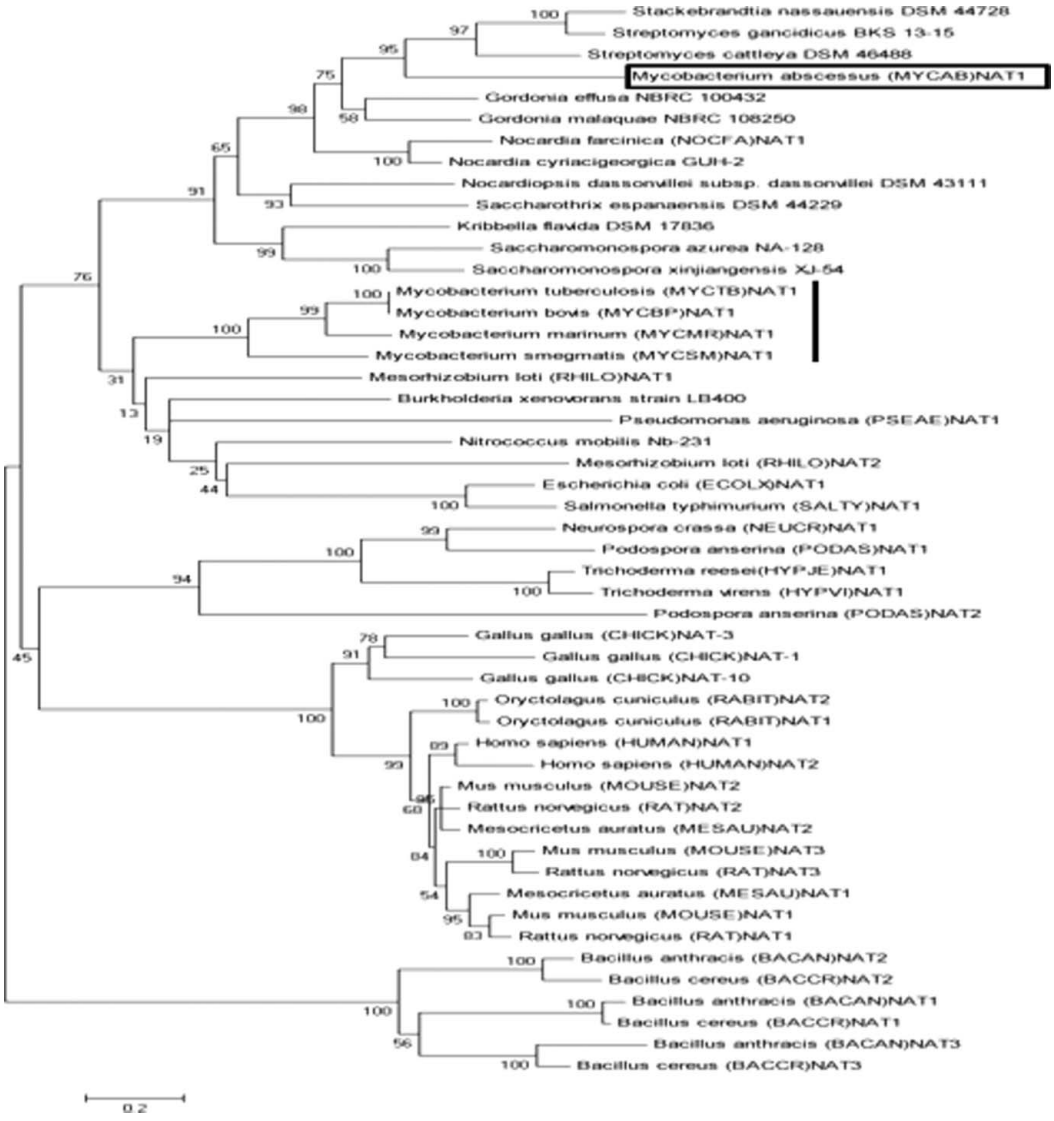

Figure 1
Phylogenetic analysis of the (MYCAB)NAT1 amino-acid sequence. The (MYCAB)NAT1 amino-acid sequence was aligned with those of characterized or putative NATs using the *MUSCLE* algorithm as implemented in *MEGA*5. The tree was obtained by the neighbour-joining method using the Dayhoff model. A total of 500 bootstrap replications were performed to determine the statistical support for clades. The mycobacterial NAT enzyme clade is shown in parentheses. The numbers indicate the probability of a phylogenetic event occurring by chance (higher probabilities are represented by lower numbers). The scale bar represents the estimated evolutionary distance.

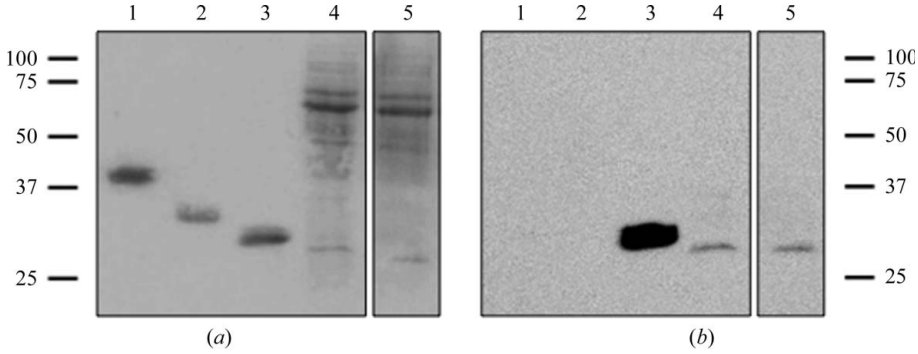

Figure 2
Expression of (MYCAB)NAT1 in *M. abscessus* R/S. (*a*) SDS–PAGE analysis of cellular extracts. 2 µg purified recombinant protein [human PON1, (PODAS)NAT1 or (MYCAB)NAT1] and 10 µg bacterial extract were subjected to SDS–PAGE under reducing conditions and stained with Ponceau Red. (*b*) Western blot analysis of bacterial extracts. Western blot analysis was conducted using a polyclonal antibody raised against the (MYCAB)NAT1 enzyme (1:5000 dilution). Human PON1 is in lane 1, (PODAS)NAT1 is in lane 2, (MYCAB)NAT1 is in lane 3, *M. abscessus* R extract (10 µg) is in lane 4 and *M. abscessus* S extract (10 µg) is in lane 5.

Typically, 35 µl cell extract was mixed with 700 µ*M* 2-AF and 1 m*M* AcCoA and the reaction was stopped with 15%(*v*/*v*) perchloric acid. Specific endogenous NAT activity was measured by quantifying the amount of acetylated 2-AF, acetylated INH and acetylated 4-AS using reversed-phase HPLC (Kromasil Eternity C18 column, Shimadzu; Cocaign *et al.*, 2013) and normalizing to the protein concentration and the AcCoA hydrolysis rate. Assays were performed in triplicate for each *M. abscessus* morphotype.

2.9. *In vivo* acetylation assays

Fresh exponential (OD at 600 nm = 0.6) phase cultures (20 ml) of *M. abscessus* morphotypes S and R were supplemented with 400 µ*M* 2-AF, INH or 4-AS. The rate of acetylation of the aromatic substrates by *M. abscessus* was measured by HPLC in the medium at different time points of incubation as described previously (Kubiak *et al.*, 2012). Experiments were performed in triplicate for each *M. abscessus* morphotype.

3. Results

3.1. Sequence analysis of (MYCAB)NAT1 reveals a significant phylogenetic distance from other mycobacterial NAT enzymes

The amino-acid sequence of (MYCAB)NAT1 shows sequence identity ranging from 20 to 43% with regard to structurally and functionally characterized NATs. (MYCAB)NAT1 possesses the consensus motifs WENL (residues 42–45) and RGGYCYE (residues 69–75) as well as the canonical Cys73, His110 and Asp125 catalytic residues previously found in NAT enzymes (Supplementary Fig. S1[1]). The sequence identities between (MYCAB)NAT1 and the mycobacterial (MYCTB)NAT1, (MYCSM)NAT1 and (MYCMR)NAT1 enzymes are 30, 34 and 31%, respectively. In comparison, the three characterized mycobacterial NATs share between 59 and 73% sequence identity. Sequence alignment suggests that (MYCAB)NAT1 is closely related to the *Nocardia farcinica* [(NOCFA)NAT1] enzyme, with 43% sequence identity. To better assess the relationship between the mycobacterial NATs, we conducted a phylogenetic analysis of the (MYCAB)NAT1 amino-acid sequence with sequences of well characterized NATs and with selected (representative strain/species) NAT sequences retrieved by *BLAST* (Fig. 1). The phylogenetic tree reveals a monophyletic clade that contains (MYCAB)NAT1 as well as (NOCFA)NAT1 and NAT sequences from *Streptomyces* and *Gordonia* species. Surprisingly, there is a clear-cut segregation of the *M. abscessus* NAT sequence from those of the other mycobacterial enzymes (MYCTB)NAT1, (MYCSM)NAT1 and (MYCMR)NAT1, which are clustered in a different clade with the other bacterial NAT sequences. Together, these results emphasize the phylogenetic distance between (MYCAB)NAT1 and the other mycobacterial NATs characterized to date and suggest possible structural and functional peculiarities of (MYCAB)NAT1.

3.2. Purification of the recombinant (MYCAB)NAT1 enzyme and development of a rabbit anti-(MYCAB)NAT1 polyclonal antibody

The ORF coding for wild-type (MYCAB)NAT1 was cloned into pET-28a and further expressed in *E. coli*. The protein was easily purified to homogeneity as a hexahistidine-tagged fusion protein, with typical yields of 4–5 mg protein per litre of culture. SDS–PAGE analysis shows a major band below the 37 kDa protein marker, consistent with the expected molecular weight of 31 kDa (Fig. 2*a*). Polyclonal antibodies against *M. smegmatis* and *M. tuberculosis* NAT failed to detect recombinant (MYCAB)NAT1 in Western blotting experiments (data not shown). This lack of cross-reactivity further supported the distance between (MYCAB)NAT1 and the other mycobacterial NAT enzymes. In order to have a tool to detect endogenous (MYCAB)NAT1 in *M. abscessus* cells, we generated a rabbit polyclonal antibody using purified recombinant (MYCAB)NAT1. As shown in Fig. 2(*b*), the (MYCAB)NAT1 antibody was able to specifically recognize the recombinant enzyme. This antibody was then used to probe the expression of (MYCAB)NAT1 in protein lysates of the rough and smooth morphotypes of *M. abscessus*. As shown in Fig. 2(*b*), similar levels of expression of (MYCAB)NAT1 were found in the bacterial extracts, thus confirming endogenous expression of the enzyme. These data are supported by

[1] Supporting information has been deposited in the IUCr electronic archive (Reference: YT5074).

microarray analyses showing similar levels of mRNA expression (data not shown).

3.3. Purified recombinant (MYCAB)NAT1 acetylates a broad range of aromatic amines including the anti-tubercular drugs 4-aminosalicylate and isoniazid

The kinetic parameters K_m^{app} and k_{cat} and the catalytic efficiency k_{cat}/K_m^{app} were determined for a set of prototypic NAT aromatic substrates (Table 2). No acetylation was observed for the four sulfonamide compounds tested which are known to be acetylated by *Bacillus anthracis* or *Legionella pneumophila* NATs (Pluvinage *et al.*, 2007; Kubiak *et al.*, 2012). In contrast to the data reported for (MYCMR)NAT1, (MYCSM)NAT1 and (MYCTB)NAT1, no acetylation of *p*ABA, an aromatic amine metabolized from folic acid, was found with (MYCAB)NAT1 (Brooke *et al.*, 2003; Fullam *et al.*, 2008; Sikora *et al.*, 2008). Aniline derivatives were readily acetylated by (MYCAB)NAT1, with catalytic efficiency values ranging from 52 560 to 244 389 M^{-1} s^{-1}. These values appeared to be slightly higher than those reported for other bacterial NATs (Kubiak *et al.*, 2012). A large difference in acetylation was observed for INH and HDZ, two arylhydrazine drugs, with the affinity of INH for (MYCAB)NAT1 being rather low (K_m^{app} = 6.75 mM) and the turnover being 18-fold lower than that of HDZ. A similar trend was observed with the other characterized mycobacterial NATs, *i.e.* (MYCMR)NAT1, (MYCSM)NAT1 and (MYCTB)NAT1 (Brooke *et al.*, 2003; Sikora *et al.*, 2008; Fullam *et al.*, 2008). Interestingly, when compared with the data obtained with recombinant (MYCTB)NAT1 (Sikora *et al.*, 2008), (MYCAB)NAT1 was more than 25 times more efficient at acetylating the anti-tubercular drug INH.

4-AS, which is also an anti-tubercular drug, was also found to be readily acetylated by (MYCAB)NAT1 but with a lower (by fivefold) catalytic efficiency when compared with INH. Differences were observed between the two positional isomers 5-AS and 4-AS, with the latter having a catalytic efficiency 283-fold lower than that of 5-AS. The arylamine 2-AF was by far the best substrate for the recombinant enzyme, with a catalytic efficiency 20-fold higher than that for 5-AS (1.36×10^6 M^{-1} s^{-1}) and with the highest affinity observed for the substrates tested (146 μM). Together, these data show that purified recombinant (MYCAB)NAT1 has significant NAT activity toward different aromatic amines, including anti-tubercular drugs. The enzyme also displays certain substrate differences from other mycobacterial enzymes.

Small inhibitor molecules have recently been developed against *M. tuberculosis* (MYCTB)NAT1 that are also potent inhibitors of (MYCSM)NAT1 and (MYCMR)NAT1 (Westwood *et al.*, 2010; Fullam *et al.*, 2013). We examined the ability of the recently developed inhibitor molecule 3-benzoyl-4-phenyl-1-methylpiperidinol (compound **1**), a piperidinol derivative, to inhibit the activity of (MYCAB)NAT1. In contrast to the data obtained with the other mycobacterial NAT enzymes, compound **1** was found to be a poor inhibitor of (MYCAB)NAT1, with an IC_{50} above 70 μM, whereas (MYCMR)NAT1 and (MYCTB)NAT1 were found to be inhibited with IC_{50} values of 1.3 and 7.7 μM, respectively (Abuhammad *et al.*, 2012). These results show that (MYCAB)NAT1 has a different behaviour towards compound **1** and further support the structural/functional peculiarities of (MYCAB)NAT1.

Table 2
(MYCAB)NAT1 kinetic parameters towards typical aromatic NAT substrates.

Specific activities were determined using the DTNB [5,5′-dithiobis-(2-nitrobenzoic acid)] assay. This test quantifies the hydrolysis rate of AcCoA (400 μM) in the presence of various concentrations of aminoaryl substrate. Kinetic parameters (k_{cat} and K_m^{app}) were obtained by non-linear fitting to the Michaelis–Menten equation. All assays were carried out in triplicate. Data are presented as the mean ± SD of three independent experiments. ND, not detectable.

Class of compound	Short name	k_{cat} (s^{-1})	K_m^{app} (μM)	k_{cat}/K_m^{app} (M^{-1} s^{-1})
Aniline derivatives				
4-Iodoaniline	4-IA	71 ± 17	1386 ± 53	596 ± 10305
4-Butoxyaniline	4-BOA	112 ± 3	462 ± 51	244389 ± 31541
3,4-Dichloroaniline	3,4-DCA	8 ± 0.8	157 ± 2	52560 ± 2195
Arylhydrazines				
Isoniazid	INH	9 ± 2	6754 ± 2009	1317 ± 123
Hydralazine	HDZ	168 ± 24	393 ± 81	434490 ± 76404
Other arylamines				
2-Aminofluorene	2-AF	199 ± 9	146 ± 7	1363312 ± 13200
4-Aminosalicylate	4-AS	1 ± 0.2	3827 ± 464	252 ± 20
5-Aminosalicylate	5-AS	47 ± 5	662 ± 77	71325 ± 2 437
para-Aminobenzoic acid	*p*ABA	ND	ND	ND
Ambroxol	ABX	ND	ND	ND
Trimethoprim	TMP	ND	ND	ND
Sulfonamides				
Sulfamethazine	SMZ	ND	ND	ND
Sulfamethoxazole	SMX	ND	ND	ND
Sulfadiazine	SDZ	ND	ND	ND
Sulfapyridine	SP	ND	ND	ND

3.4. (MYCAB)NAT1 is endogenously expressed and functional in both the rough and the smooth morphotypes of *M. abscessus*

As stated above, (MYCAB)NAT1 is expressed at both mRNA and protein levels in the rough and smooth forms of *M. abscessus*. To assess whether endogenous (MYCAB)NAT1 displays NAT activity, we incubated lysates of the rough and smooth morphotypes of *M. abscessus* with 700 μM 2-AF, which was found to be the best aromatic amine substrate of the purified recombinant form. *N*-Acetylation of 2-AF by endogenous activity was measured by HPLC as described previously (Kubiak *et al.*, 2012). The acetylated product was readily detected in time-dependent, protein-dependent and AcCoA-dependent manners with acetylation rates of 1.42 ± 0.3 and 2.03 ± 0.04 nmol min^{-1} mg^{-1} of protein in rough and smooth extracts, respectively. Acetylation of INH and 4-AS by the lysates was also detected but at much lower rates (with similar values for R and S morphotypes and ranging from 0.01 to 0.05 nmol min^{-1} mg^{-1} for 4-AS and INH, respectively).

We further analyzed the endogenous acetylation of 2-AF, INH and 4-AS by growing *M. abscessus* R and S morphotypes in the presence of these aromatic compounds and measuring

their *N*-acetylated form in the culture medium. In accordance with the data obtained with the extracts, we found that acetylated 2-AF and INH were readily detected in the culture medium of both the R and the S morphotypes. The rate of endogenous acetylation of 2-AF was 130 ± 30 and 150 ± 20 pmol min^{-1} per millitre of culture for the S and the R morphotypes, respectively. The rates of acetylation of INH were found to be lower (4.5 ± 1.2 and 2.2 ± 0.5 pmol min^{-1} per millitre of culture for the S and the R morphotypes, respectively), which is in agreement with the results obtained with the recombinant enzymes and with bacterial extracts. As expected, the endogenous acetylation of 4-AS was low (<0.5 pmol min^{-1} per millitre of culture). Together, these results demonstrate that (MYCAB)NAT1 is functional in both morphotypes of *M. abscessus* (with similar activities) and can endogenously modify aromatic amines such as INH.

3.5. Crystal structure of (MYCAB)NAT1: differences in the solvent-exposed and CoA-binding site loops

The 1.8 Å resolution crystal structure of (MYCAB)NAT1 (Table 1) was obtained from a single hit in the original screen (15% PEG 6000, 5% glycerol). The asymmetric unit consisted of a tetramer and belonged to the monoclinic space group *C*121. Clear electron density was observed for all 278 residues of the enzyme and for six residues of the thrombin cleavage

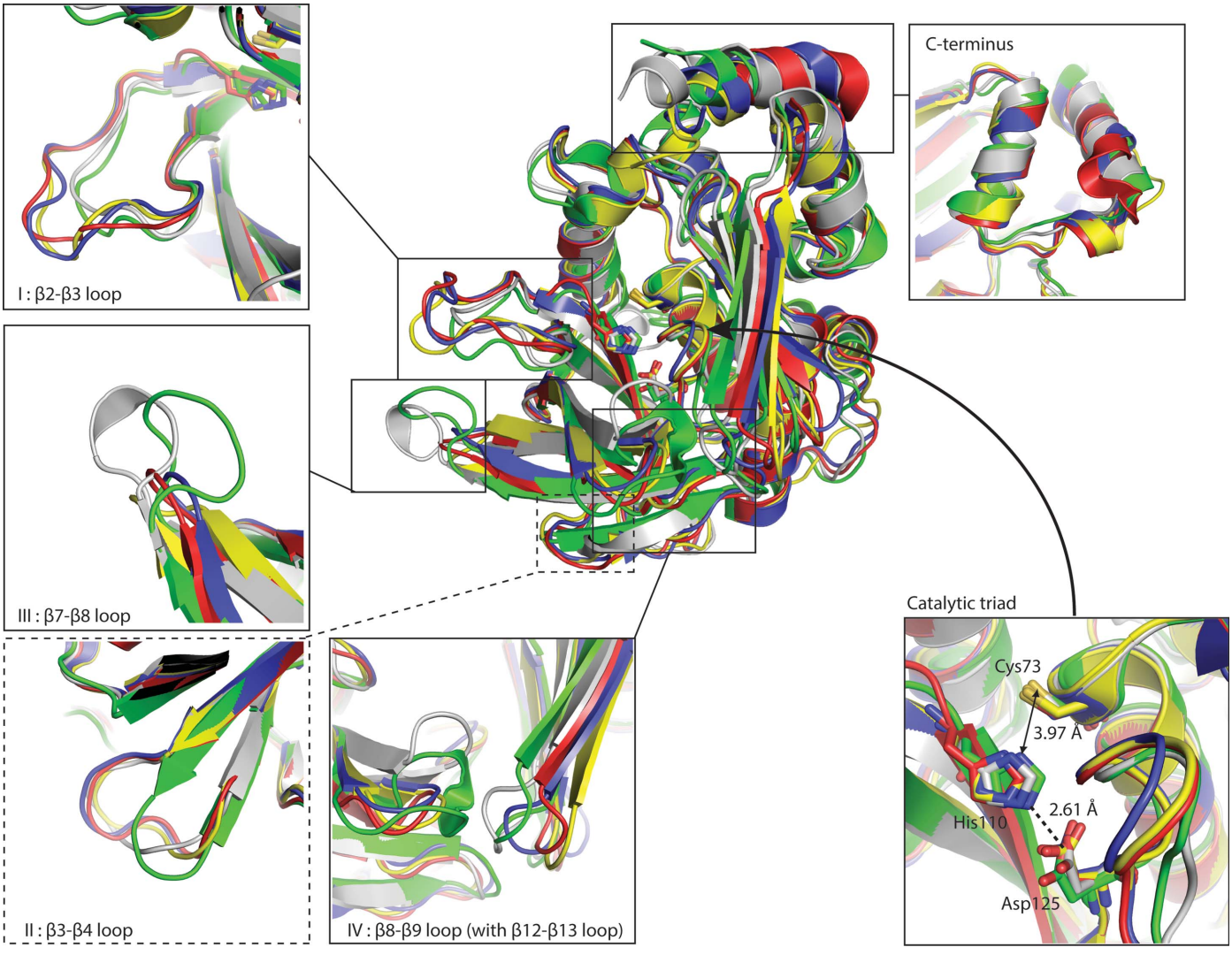

Figure 3
Comparison of the overall structure of (MYCAB)NAT1 with those of all crystallized mycobacterial NAT enzymes. The 1.8 Å resolution structure of (MYCAB)NAT1 (green) was aligned with the NAT structures from *M. smegmatis* [(MYCSM)NAT1, yellow, PDB entry 1w6f], *M. marinum* [(MYCMR)NAT1, blue, PDB entry 3ltw], *M. tuberculosis* [(MYCTB)NAT1, red, PDB entry 4bgf] and *N. farcinica* [(NOCFA)NAT1, white, PDB entry 3d9w] using *PyMOL*. The four loops showing significant divergence in (MYCAB)NAT1 are emphasized by squares and an enlarged panel is shown for each region: region I between strands β2 and β3 (residues 99–109), region II between strands β3 and β4 (residues 118–119), region III between strands β7 and β8 (residues 157–163), region IV between strands β8 and β9 (residues 171–178) and the C-terminal helix α11. Region II is shown in dots as it is in the background. All residues are numbered according to the (MYCAB)NAT1 sequence. Catalytic triads were also superimposed (lower right panel): the triad geometry is conserved, although the catalytic His is hydrogen-bonded to the OD1 atom of the catalytic Asp in both (MYCAB)NAT1 and (NOCFA)NAT1. Distances are shown in Å and hydrogen bonds as dotted lines.

site [Val(−5)-Pro(−4)-Arg(−3)-Gly(−2)-Ser(−1)-His0]. The high-resolution structure of (MYCAB)NAT1 reveals the canonical three-domain NAT fold: an α-helical bundle (1–89), a β-barrel (90–191) and an α/β lid (192–278) (Kubiak, Dairou *et al.*, 2013; Kubiak, Li de la Sierra-Gallay *et al.*, 2013). The catalytic residues Cys73, His110 and Asp125 have well defined electron densities and form the canonical catalytic triad. Superimposition with the catalytic triad of mycobacterial NATs shows 1.2 and 0.95 Å shifts (measured at C^{γ}; Fig. 3). In particular, the catalytic Cys–His and His–Asp distances are similar, but the Cys73–Asp125 distance is 1.45 Å longer in (MYCAB)NAT1 compared with the equivalent catalytic triad residues in the other mycobacterial NATs (Supplementary Fig. S2*a*). *N. farcinica* (NOCFA)NAT1 was found to be the structurally closest relative of (MYCAB)NAT1, with an r.m.s.d. value of 1.020 Å over 278 amino acids, compared with values of 1.639, 1.684 and 1.793 Å over 260 residues for (MYCTB)NAT1, (MYCMR)NAT1 and (MYCSM)NAT1, respectively (Supplementary Table S1). In addition, both (MYCAB)NAT1 and (NOCFA)NAT1 have a similar geometry which differs from those of the other mycobacterial NATs in that the catalytic His residue is hydrogen-bonded to the OD1 (instead of the OD2) O atom of the catalytic Asp (Fig. 3). Moreover, the catalytic Asp residue of (MYCAB)NAT1 and (NOCFA)NAT1 both form a hydrogen bond to a residue localized on β-strand β9 (His183 and Arg190, respectively). In contrast, the catalytic Asp interacts with Asn74, which is localized on an α-helix (α5) in the other mycobacterial NATs (data not shown). Four regions involved in the regulation of NAT activity show a significant difference in (MYCAB)NAT1 compared with the other mycobacterial NATs: the β2–β3 loop is three residues shorter (region I; 99–109), the β3–β4 loop is two residues shorter (region II; 118–119), the β7–β8 loop is five residues longer (region III; 157–163) and the β8–β9 loop is five residues longer (region IV; 171–178). Region III also forms a helical turn in contrast to an unorganized loop in other NAT enzymes (Fig. 3, Supplementary Fig. S1). Similar differences in regions I, III and IV are observed in (NOCFA)NAT1, although region II is closer to those of the other mycobacterial NAT enzymes (Fig. 3). Furthermore, the C-terminal helix of (MYCAB)NAT1 and (NOCFA)NAT1 is significantly longer than the C-terminal helix of mycobacterial NATs: it consists of three complete helical turns, compared with the 1.5–2 turns found in the other NATs. These differences seem to be owing to improved organization of the N-terminal part of helix α11 in (MYCAB)NAT1 (Fig. 3). The binding-pocket volume of (MYCAB)NAT1 (818 $Å^3$) is similar to those of (NOCFA)NAT1 (961 $Å^3$) and (MYCSM)NAT1 (1044 $Å^3$) but is two and 2.5 times smaller than those of (MYCTB)NAT1 and (MYCMR)NAT1 (1506 and 2139 $Å^3$, respectively; Fig. 4). Moreover, the electrostatic charge of the binding pocket was mapped and suggests that the binding pocket of (MYCAB)NAT1 has slightly more negative electrostatic charge compared with the other mycobacterial NAT enzymes, with (MYCTB)NAT1 showing a clearly positively charged binding pocket as observed for (NOCFA)NAT1 (Fig. 4).

3.6. Docking studies of aromatic amine substrates and compound 1

Based on the solved high-resolution structure, we generated ligand-annealing models of several substrates of interest (INH, 4-AS, HDZ, 2-AF, 4-IA and 4-BOA; see Table 2) to the Cys73-acetylated intermediate of (MYCAB)NAT1. The binding energies estimated from molecular docking were in

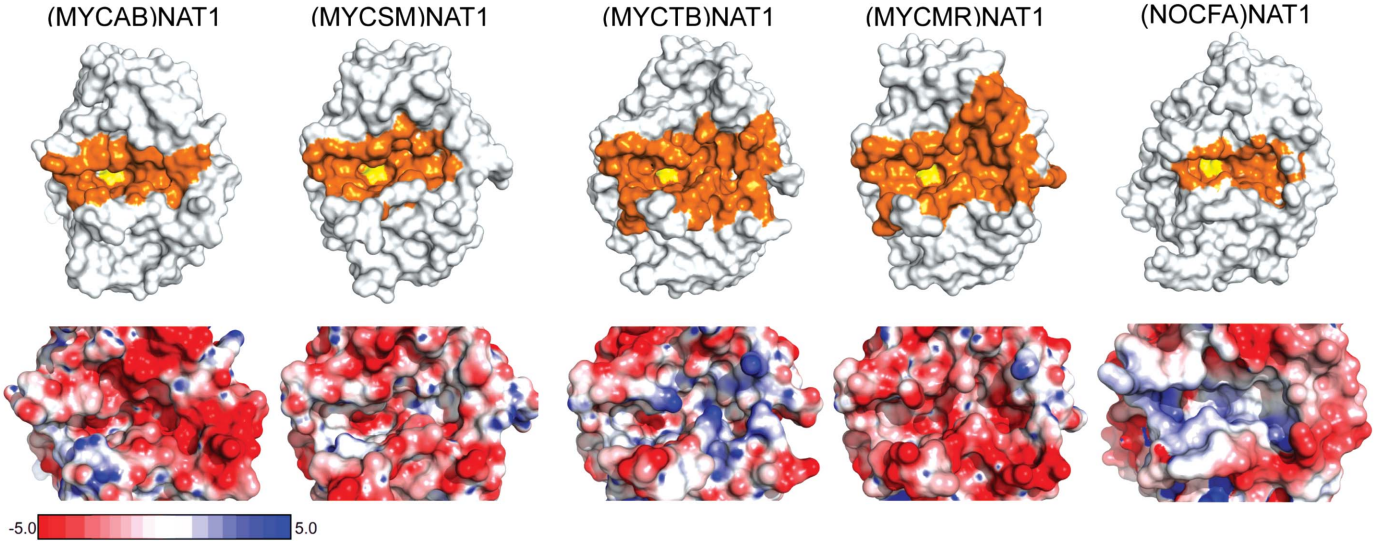

Figure 4
The binding pocket of (MYCAB)NAT1. Binding-pocket properties of the fast-growing mycobacterial NATs (MYCAB)NAT1 and (MYCSM)NAT1, the slow-growing mycobacterial NATs (MYCTB)NAT1 and (MYCMR)NAT1 and the non-mycobacterial (NOCFA)NAT1 are shown. The binding cavities (upper row) were calculated using *CastP* and are shown as orange surfaces. The catalytic cysteine is coloured yellow for orientation of the binding pocket. The electrostatic charge properties of the binding cavities are shown in the lower row, with the scale bar indicating positive (blue) and negative (red) charge.

good agreement with the K_m^{app} values reported in Table 2 (Supplementary Fig. S3) and are as follows: INH > 4-AS > 4-IA > 4-BOA > HDZ > 2-AF (Supplementary Fig. S3). However, the mode of binding of the different substrates is very similar and interactions are mainly achieved with the hydrophobic residues Trp42, Val98, Met100, Phe128, Phe210 and Phe215 (Fig. 5*a*). All aromatic amines tested appear to form a hydrogen bond between the amino group and the catalytic His110 residue and with the carboxyl O atom of Gly127, and 4-AS forms an extra hydrogen bond between its 2-hydroxyl O atom and the amino group of Gly127. Thus, docking suggests that substrates are mostly stabilized through van der Waals interactions. When compared with the crystallized INH–(MYCSM)NAT1 and HDZ–(MYCMR)NAT1 complexes (which are the two mycobacterial NAT enzymes crystallized with a substrate to date), there is a 2.9 and 2.5 Å shift of the substrate out of the binding pocket, most likely owing to the acetyl group on the catalytic cysteine (Fig. 5*b*). In both models, HDZ has a very similar orientation, although the amine group is rotated towards the free cysteine in (MYCMR)NAT1, while it is in the plane of the phthalazine ring in (MYCAB)NAT1. In contrast, INH is rotated almost 180° around the *para* axis of its phenyl ring in (MYCAB)NAT1 compared with (MYCSM)NAT1, again to fulfill the amine–Gly127 hydrogen bond.

We also carried out docking studies with compound **1**, which was found to be a poor inhibitor of (MYCAB)NAT1 (see above). The docking of compound **1** in (MYCAB)NAT1 was somewhat easier to achieve than in (MYCMR)NAT1 and (MYCTB)NAT1, although the inhibitor was designed and selected for the latter two enzymes. Of the 100 rotamers docked in (MYCAB)NAT1, 96 had a very similar orientation, with only minor changes in the substituent orientations. Conversely, in (MYCMR)NAT1 and (MYCTB)NAT1, four out of 100 and five out of 150 main rotamers could be identified (Fig. 6*a*). These results suggest that compound **1** is more anchored (less dynamic) in the binding pocket of (MYCAB)NAT1 than in the two other mycobacterial NATs.

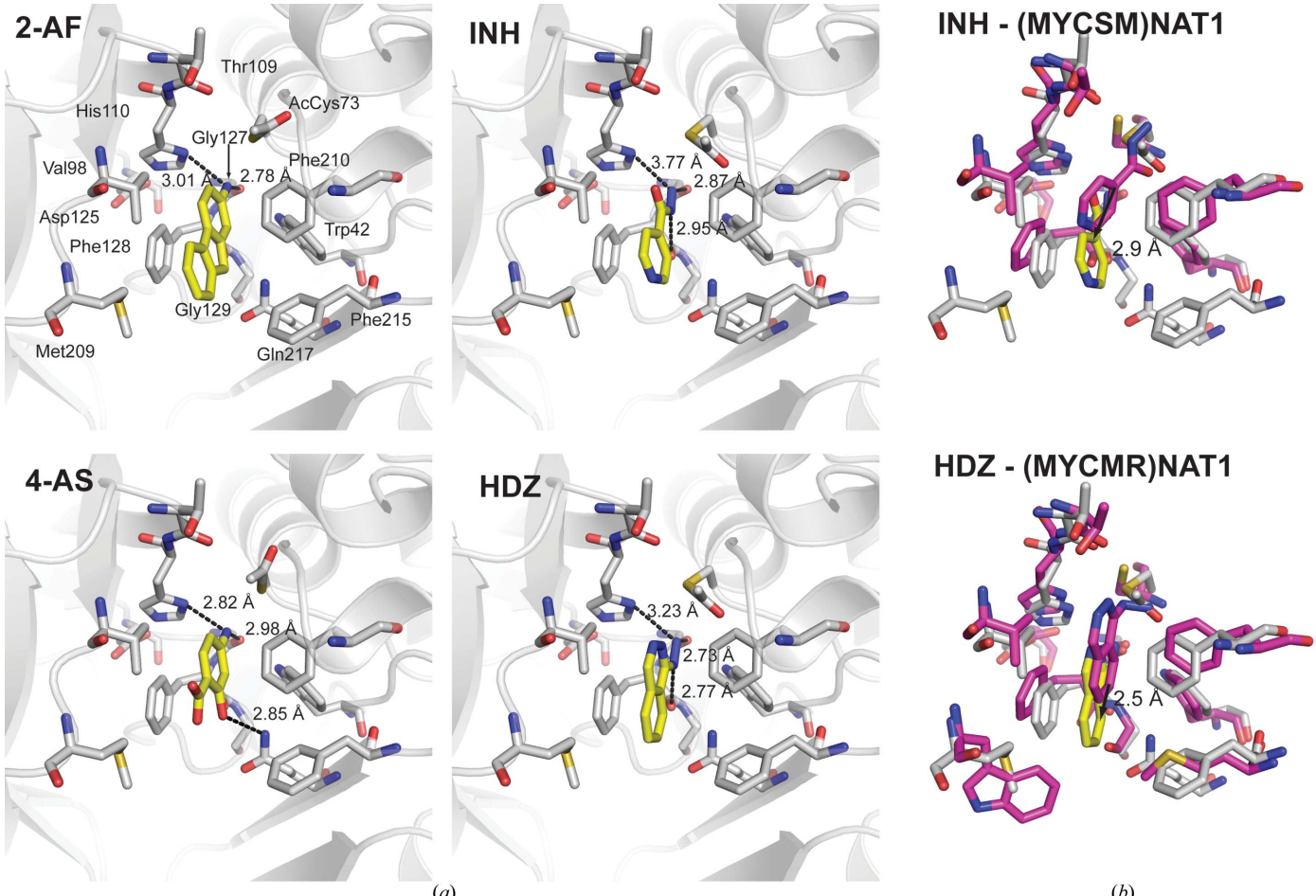

Figure 5
Docking of 2-AF, 4-AS, INH and HDZ to (MYCAB)NAT1. (*a*) The structure of (MYCAB)NAT1 was used as a template to generate a model of the acetylated intermediate of the enzyme (Ac-Cys73) to which 2-AF, 4-AS, INH and HDZ molecules were docked using *rDock*. Catalytic residues and residues interacting with the substrates are indicated in white sticks and the docked molecule is coloured yellow. Hydrogen bonds are shown as black dotted lines with their lengths labelled. (*b*) Comparison of the binding modes of INH and HDZ in the modelled (MYCAB)NAT1, (MYCSM)NAT1 (complexed with INH; PDB entry 1w6f) and (MYCMR)NAT1 (complexed with HDZ; PDB entry 3ltw). For both complexed structures the residues reported to interact with the bound substrate are shown in magenta. The arrow indicate the relative displacement (in Å) of substrate between substrate-bound structures and the substrate docked to the acetylated model of (MYCAB)NAT1 (white sticks). Structures were aligned in *PyMOL*.

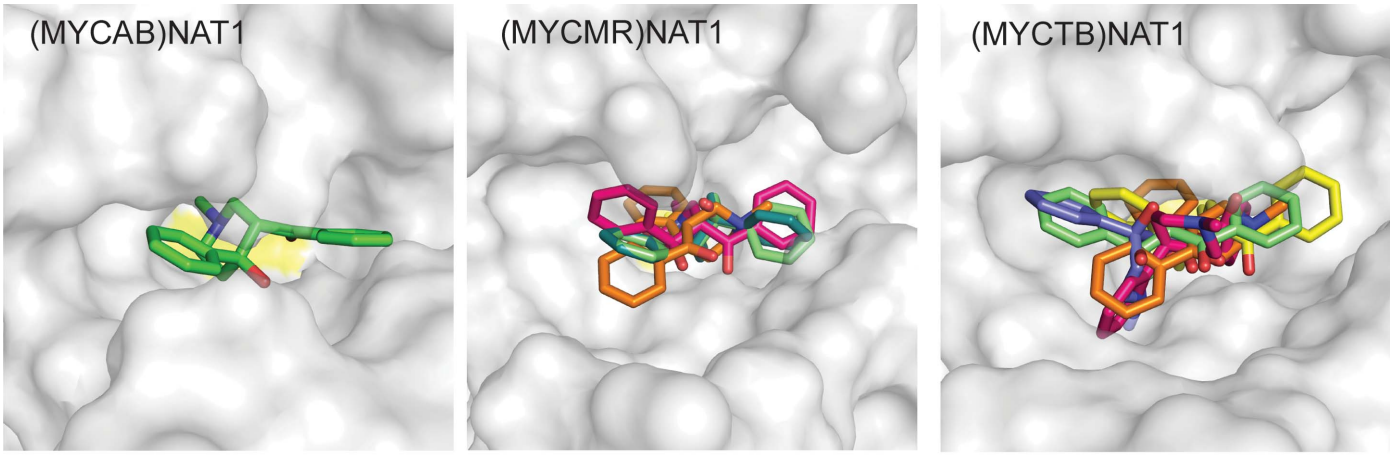

(*a*)

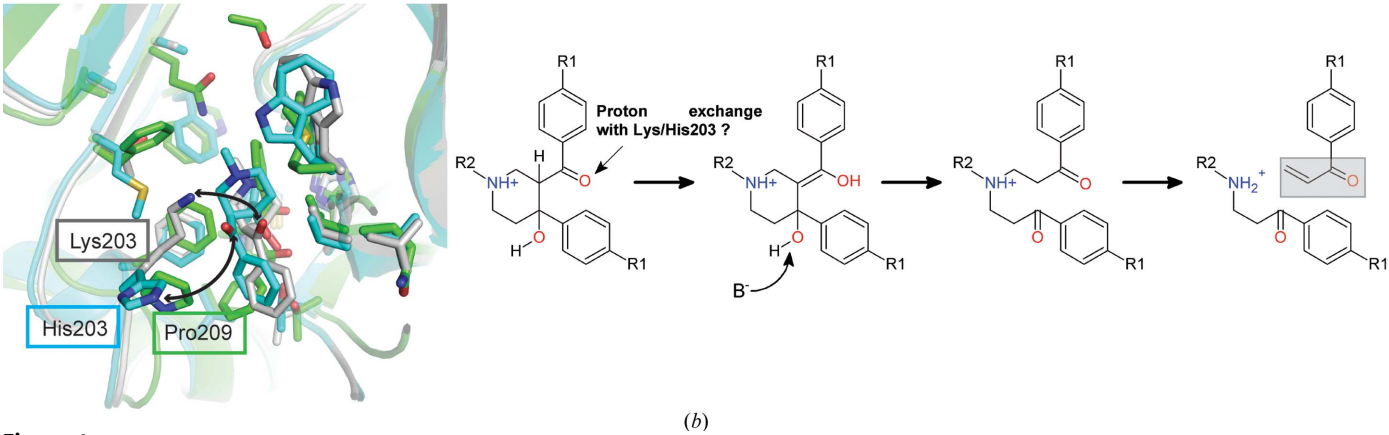

(*b*)

Figure 6
Mode of binding and suggested mechanism of action for compound **1** in (MYCAB)NAT1. (*a*) Compound **1** was docked to the unacetylated form of (MYCAB)NAT1, (MYCTB)NAT1 and (MYCMR)NAT1 as previously described in Fig. 5. All proteins are in the same orientation, with the catalytic cysteine coloured yellow. For (MYCTB)NAT1 and (MYCMR)NAT1, the most frequent rotamers observed in the docking are shown in different colours, with O atoms in red and N atoms in blue. For (MYCAB)NAT1, a single rotamer is indicated as it corresponds to 95% of the rotamers observed upon docking. (*b*) Suggested mechanism for the activation of compound **1** to the inhibitory molecule PVK. Superimposition of the residues within a distance of 4 Å of compound **1** in each structure is shown (left). Compound **1** was suggested to undergo a β-elimination causing the formation of a reactive PVK molecule: we propose that this β-elimination is owing to a proton exchange between the O atom of the benzoyl moiety of compound **1** and a residue that could be either Lys203 or His203 in (MYCTB)NAT1 and (MYCMR)NAT1, respectively (right). The absence of a protonatable residue at this position could be responsible for the absence of inhibition of (MYCAB)NAT1.

The residues forming the binding pocket of compound **1** are highly conserved, and most are identical to those involved in the binding of aromatic amine substrates, with a few additional residues. In (MYCAB)NAT1 these residues are Gln99, Gly129, Thr130, Val202, Pro209 and Val216. The two main differences are the change of Phe215 and Pro209 in (MYCAB)NAT1 to Met209 and His203 in (MYCMR)NAT1 and to Thr209 and Lys203 in (MYCTB)NAT1.

4. Discussion

Despite its striking public health importance, the biochemistry of *M. abscessus* is poorly documented, with few proteins described both structurally and functionally (Soroka *et al.*, 2014). Most of the known metabolic pathways have been inferred from the recently fully sequenced genome (Ripoll *et al.*, 2009) and most studies have focused on the improvement of detection methods (Rolfe *et al.*, 2013). Although the major threat posed by *M. abscessus* is mainly owing to its resistance to antibiotics, the structural and functional characterization of enzymes that could modify/neutralize antibiotics is poorly documented (Nessar *et al.*, 2012).

In the present paper, we report the functional characterization and the 1.8 Å high-resolution structure of the arylamine *N*-acetyltransferase (MYCAB)NAT1 from *M. abscessus*. This family of enzymes is known to metabolize and inactivate aromatic chemicals, including antibiotics (Sim *et al.*, 2012). Phylogenetic analysis suggested that the enzyme is phylogenetically distant from other mycobacterial NAT enzymes characterized to date. (MYCAB)NAT1 was indeed found to be closely related to NAT enzyme orthologues from *Streptomyces* and *Gordonia* and to the structurally characterized (NOCFA)NAT1 from *N. farcinica*. These data are in agreement with previous genomic analyses, which showed important horizontal gene-transfer events mostly from actinobacteria (*e.g. Streptomyces* sp.; Ripoll *et al.*, 2009). Inter-

estingly, most of these genes were predicted to be involved in the metabolism of aromatic compounds (Ripoll *et al.*, 2009). In addition, the genomic organization of the *nat* gene in *M. abscessus* is substantially different from that of other slow- and fast-growing bacteria in that it is not part of an operon (Sim, Sandy *et al.*, 2008). These data suggested that the *nat* gene enzyme from *M. abscessus* might have been acquired through horizontal transfer (Martins *et al.*, 2008) and suggest differences from other mycobacterial NATs. These differences were further supported by the absence of cross-reactivity of the recombinant (MYCAB)NAT1 with antibodies raised against (MYCSM)NAT1 and (MYCTB)NAT1.

The purified recombinant (MYCAB)NAT1 catalyzed the AcCoA-dependent acetylation of several aromatic amines including arylamine antibiotics, thus indicating that the enzyme was functional. Moreover, the enzyme was found to display a typical (HUMAN)NAT1-like substrate specificity similar to other bacterial NATs, with 2-AF and 5-AS being the best substrates and the enzyme not being able to acetylate the folate catabolite *p*ABA (Deloménie *et al.*, 2001). Our data are in agreement with previous observations made with other bacterial NAT enzymes, which were found to be able to acetylate 4-AS but not *p*ABA, despite the very small difference between these two chemicals. A study based on docking calculations on (MYCSM)NAT1 has suggested that 4-AS and *p*ABA bind identically. However, in contrast to *p*ABA, 4-AS possesses a hydroxyl chemical group on the aromatic ring that forms a hydrogen bond to the Thr109 residue in the active site. The absence of this hydrogen bond between *p*ABA and Thr109 results in an decreased affinity for *p*ABA compared with 4-AS (Sandy *et al.*, 2005). In (MYCAB)NAT1, docking of 4-AS into the acetylated form of the enzyme predicts that 4-AS is hydrogen-bonded to residue Gln217 *via* the OH function that is missing in *p*ABA. Thus, in accordance with Sandy *et al.* (2005), it is likely that this missing interaction is critical enough to impair the acetylation of *p*ABA by (MYCAB)NAT1.

The range of catalytic efficiencies for aromatic amine substrates is rather broad (10^2–10^6 M^{-1} s^{-1}), but is within the average range of values observed for other bacterial NATs (Sikora *et al.*, 2008; Kubiak *et al.*, 2012). The substrate specificity is close to those of other mycobacterial NAT enzymes (Sikora *et al.*, 2008; Fullam *et al.*, 2008). Both anti-tubercular agents, INH and 4-AS, were found to be readily acetylated by (MYCAB)NAT1 but with lower efficiencies (1.3×10 and 2.5×10^2 M^{-1} s^{-1} for INH and 4-AS, respectively). The values of these efficiencies are mainly owing to a low affinity (6.7 and 3.8 m*M* for INH and 4-AS, respectively). In this regard, the (MYCAB)NAT1 enzyme is closer to the (MYCTB)NAT1 enzyme (K_m^{app} for INH equal to 100 m*M*) than to the two other enzymes (MYCSM)NAT1 and (MYCMR)NAT1, for which the affinity was reported to be lower than 25 µ*M* (Fullam *et al.*, 2009; Sandy *et al.*, 2005; Sikora *et al.*, 2008; Payton *et al.*, 1999). However, it is important to bear in mind that differences in the experimental conditions (*e.g.* the AcCoA concentration) might impact on the kinetic parameters reported. Nonetheless, under similar conditions (Sikora *et al.*, 2008), (MYCAB)NAT1 is 25-fold more efficient at acetylating INH than (MYCTB)NAT1. The docking of substrates to the structure of (MYCAB)NAT1 matches the affinities measured in steady-state kinetics well. We found that the 2-AF, 4-AS, INH, HDZ, 4-BOA and 5-AS substrates are all stabilized by a network of van der Waals interactions with hydrophobic residues (Trp42, Val98, Met100, Phe128, Phe210 and Phe215) that are highly conserved throughout all bacterial NAT enzymes and this is not of much help in explaining the different binding affinities between substrates in (MYCAB)NAT1. Although similar residues are involved in the binding of INH in (MYCAB)NAT1, (MYCSM)NAT1 and (MYCMR)NAT1, the substrate is rotated by 180° around the *para* axis of its phenyl ring. Furthermore, we conducted docking with the acetylated form of the enzyme, which is most likely to be the molecular entity that will bind the substrate during the ping-pong bi-bi mechanism (Weber & Cohen, 1967), leading to an outward shift of 2.5 and 2.9 Å of INH and HDZ, respectively. In these models, the substrate amine extremity forms a hydrogen bond to Gly127 and Cys73. However, the latter is unlikely to occur as the amine function is more prone to undergo nucleophilic attack by the catalytic Cys73 residue. Nevertheless, our results add to the general idea obtained from docking models and substrate-bound structures that all aromatic amines have a very similar mode of binding that can still be specifically modulated by binding-pocket residues. Interestingly, Arg115 in (NOCFA)NAT1 was suggested to be responsible for the weak affinity towards INH compared with (MYCSM)NAT1, which has a Pro at this position (Martins *et al.*, 2008). Although an Arg residue is also found in (MYCAB)NAT1, it is more than 10 Å from the docked INH molecule and thus is unlikely to be responsible for the difference in affinity observed compared with other mycobacterial NATs.

(MYCAB)NAT1 adopts the canonical three-domain NAT fold forming a Cys73–His110–Asp125 catalytic triad responsible for the acetylation reaction (Kubiak, Dairou *et al.*, 2013; Kubiak, Li de la Sierra-Gallay *et al.*, 2013). Nevertheless, compared with other mycobacterial NATs, (MYCAB)NAT1 harbours noticeable changes in four loop regions linking β-strands β2 and β3 (region I; 99–109), β3 and β4 (region II; 118–119), β7 and β8 (region III; 157–163), and β8 and β9 (region IV; 171–178) that resemble those observed in (NOCFA)NAT1 (except for region II). Region I has been suggested to alter the accessibility to the binding pocket in (RHILO)NAT1 (Holton *et al.*, 2005). Similarly, region IV and the proximal β12–β13 loop seem to reduce the binding-pocket accessibility in (MYCAB)NAT1 and (NOCFA)NAT1 compared with the other mycobacterial NATs (Fig. 3). Both regions I and IV are directly involved in the binding of AcCoA (Fullam *et al.*, 2008). Regions III and IV are also flanking a β-strand that interacts *via* hydrogen bonding with the CoA cofactor (Fullam *et al.*, 2008). No particular role has been found for region II (which is only composed of two amino acids). The structural differences in these regions could thereby account for the differences in kinetic parameters and substrate specificity observed in (MYCAB)NAT1 compared with the other mycobacterial NAT enzymes (Fullam *et al.*,

2008; Pluvinage *et al.*, 2011). Interestingly, the binding pockets in the NATs from the fast-growing *M. abscessus* and *M. smegmatis* as well as that from *N. farcinica* are approximately two times smaller than those found in the NATs from the slow-growing *M. marinum* and *M. tuberculosis*. In contrast, no such correlation could be established between the bacterial growth rate and the electrostatic potential of the binding cavity. Thus, although some differences still exist between (MYCAB)NAT1 and (NOCFA)NAT1, several structural features (catalytic triad geometry, binding-pocket volume and the organization of the loops involved in cofactor binding) support the phylogenetic relationship between the two orthologues and a partial divergence of (MYCAB)NAT1 from other mycobacterial NATs. In summary, it is likely that a combination of binding-pocket volume, dynamics and electrostatic charge account for the substrate-specificiy differences, which a simple docking model is unlikely to fully explain.

Although the roles of the prokaryotic NAT enzymes are unclear, these enzymes are generally considered to play a role in the environmental adaptation of the microorganism through the biotransformation of aromatic amine compounds (Boukouvala & Fakis, 2005; Pluvinage *et al.*, 2007; Kubiak *et al.*, 2012; Sim *et al.*, 2012). In addition to the steady-state kinetic analysis of recombinant (MYCAB)NAT1 using several aromatic substrates, we found that the enzyme was expressed and functional in extracts from the rough and smooth morphotypes of *M. abscessus*. More importantly, HPLC analyses of the culture media of both morphotypes showed that INH and to a lesser extent 4-AS were acetylated *in vivo* by *M. abscessus*. *M. abscessus* has not been reported to be sensitive to INH. Based on data obtained in *M. tuberculosis*, it has been suggested that the *M. abscessus whiB7* gene could be responsible for INH resistance (Nessar *et al.*, 2012). *M. tuberculosis* NAT has been shown to acetylate INH and increased expression of the enzyme results in increased INH resistance (Payton *et al.*, 1999). In addition, knock-out of the *nat* gene in *M. smegmatis* and *M. bovis* increases the sensitivity of these strains to INH (Bhakta *et al.*, 2004). Although the biological relevance of (MYCAB)NAT1 was not assessed in our study, it cannot be ruled out that the enzyme could contribute to the detoxification of toxic aromatic chemicals, including INH. Interestingly, analysis of the *M. abscessus* genome revealed the unexpected presence of many genes that are putatively involved in the metabolism of aromatic compounds (Ripoll *et al.*, 2009). Moreover, knock-out studies in *M. bovis* have revealed the key role of the NAT enzyme in the metabolism of essential mycolic lipids (Bhakta *et al.*, 2004). Further studies are needed to decipher the role that (MYCAB)NAT1 may play in *M. abscessus*. However, there is currently a lack of 'simple' genetic tools available in *M. abscessus* (Nessar *et al.*, 2012).

Several studies have indicated that NAT enzymes could be attractive therapeutic targets for the development of anti-mycobacterial compounds (Sim *et al.*, 2012). These studies have led to the development of potent inhibitors of the *M. tuberculosis*, *M. marinum* and *M. smegmatis* NATs (Westwood *et al.*, 2010; Fullam *et al.*, 2013). The similar expression and activity of (MYCAB)NAT1 in both the rough and smooth morphotypes of *M. abscessus* tends to support a basal endogenous role. Thus, in an effort to investigate a putative endogenous role of (MYCAB)NAT1 in *M. abscessus*, we tested the ability of the recently developed piperidinol compound **1** to inhibit the enzyme (Abuhammad *et al.*, 2012). Unfortunately, in our hands no significant inhibition of (MYCAB)NAT1 was observed. Although the impact of compound **1** on (MYCAB)NAT1 remains elusive, its behaviour is indisputably different when compared with other mycobacterial NAT enzymes.

Efforts to explain these differences through docking studies were only partly fruitful. The number of rotamers adopted by compound **1** suggests a much more restrained mobility when docked to (MYCAB)NAT1 compared with (MYCMR)NAT1 and (MYCTB)NAT1. This is consistent with a smaller binding pocket in (MYCAB)NAT1. The docking experiments do not fully explain the weak inhibitory effect of compound **1** since the docking shows stronger affinity towards (MYCAB)NAT1 than other mycobacterial NATs. This apparent discrepancy may come from the fact that the docking experiments did not consider factors such as hydration, protein flexibility and entropy. In addition, the lack of inhibition of (MYCAB)NAT1 by compound **1** may not be owing to binding of the molecule to the enzyme but rather owing to the fact that the microenvironment within the (MYCAB)NAT1 active site does not allow the activation of compound **1**. Indeed, the mechanism of action of the inhibitor remains elusive. However, the inhibitor has been suggested to undergo a β-elimination leading to the formation of a reactive PVK species that alkylates the catalytic cysteine, thereby irreversibly inhibiting the enzyme (Abuhammad *et al.*, 2013). However, no further precision has been suggested for the β-elimination reaction. The inability of compound **1** to inhibit the human NAT enzymes suggests that the β-elimination is likely to rely on the reaction with a residue lying in the binding pocket, *e.g. via* proton exchange between this residue and the O atom of the benzoyl moiety. Our docking studies suggest that only Lys203 in (MYCTB)NAT1 and His203 in (MYCMR)NAT1 could fulfill this proton-exchange role. Interestingly, there is a Pro at the corresponding position in (MYCAB)NAT1 (Fig. 6*b*). Altogether, the absence of a protonatable residue in the binding pocket and the single conformation of compound **1** are reasonable clues to explain the inability of the piperidinol compound to inhibit (MYCAB)NAT1. It is noteworthy that *Pseudomonas aeruginosa* (PSEAE)NAT1 and *Salmonella typhimurium* (SALTY)NAT1 are completely inhibited by 30 μM compound **1** although they possess a Val at the position of interest: still, it is possible that other residues might be responsible for the activation of the inhibitor depending on the NAT species. Finally, our results show that if (MYCAB)NAT1 were to be considered as an important enzyme for the biology of *M. abscessus*, the development of a specifically designed inhibitor will be necessary, assisted by the high-resolution structure of (MYCAB)NAT1 described in the present article.

Altogether, our functional and structural data confirm the peculiarity of *M. abscessus* (MYCAB)NAT1 with regard to other mycobacterial NATs. Differences in the effect of inhibitory compounds between the *M. tuberculosis* and the *M. abscessus* enzymes have already been reported, although to a lower extent than those that we report (Sohn *et al.*, 2008). As stated above, (MYCAB)NAT1 is phylogenetically distant from other mycobacterial NATs. The phylogenetic distance between mycobacterial NATs observed reflects the ribosomal small subunit 16S sequence-based classification (Tortoli, 2003). Such a phylogenetic distance might explain, at least in part, the inability of compound **1** to efficiently inhibit (MYCAB)NAT1. Although no clues are added here suggesting that this NAT enzyme is necessary for the bacteria in its growth or metabolic pathways, (MYCAB)NAT1 could be a potentially interesting target for the design of inhibitors. For such an experiment the present biochemical and structural analysis of (MYCAB)NAT1 is essential for the clear screening of lead compounds.

In conclusion, this study reports the first functional and structural characterization of an antibiotic-modifying enzyme from *M. abscessus*, (MYCAB)NAT1. It provides bases to better understand the substrate/inhibitor-binding specificities among mycobacterial NAT enzymes and to identify/optimize specific inhibitors. This study should also contribute to the understanding of the mechanisms responsible for the pathogenicity and extensive chemotherapeutic resistance of *M. abscessus*.

This work was supported by the Université Paris Diderot, the Institut Pasteur Paris, the Centre National de la Recherche Scientifique (CNRS) and the French Infrastructure for Integrated Structural Biology (FRISBI) ANR-10-INSB-05-01. AC and XK were supported by a PhD fellowship from the Université Paris Diderot (Ecole Doctorale B3MI). XX was supported by a PhD fellowship from the China Scholarship Council (CSC). We also acknowledge the SLS synchrotron (Villigen, Switzerland) for the provision of synchrotron-radiation facilities and we would like to thank Meitian Wang for assistance with the use of beamline X06DA. We acknowledge the 'Bioprofiler' platform for provision of HPLC facilities. We would like to thank Professor Edith Sim (Oxford University and Kingston University) for the kind gift of compound **1** and helpful discussions.

References

Abuhammad, A., Fullam, E., Lowe, E. D., Staunton, D., Kawamura, A., Westwood, I. M., Bhakta, S., Garner, A. C., Wilson, D. L., Seden, P. T., Davies, S. G., Russell, A. J., Garman, E. F. & Sim, E. (2012). *PLoS One*, **7**, e52790.

Abuhammad, A., Lowe, E. D., McDonough, M. A., Shaw Stewart, P. D., Kolek, S. A., Sim, E. & Garman, E. F. (2013). *Acta Cryst.* D**69**, 1433–1446.

Bhakta, S., Besra, G. S., Upton, A. M., Parish, T., Sholto-Douglas-Vernon, C., Gibson, K. J., Knutton, S., Gordon, S., DaSilva, R. P., Anderton, M. C. & Sim, E. (2004). *J. Exp. Med.* **199**, 1191–1199.

Boukouvala, S. & Fakis, G. (2005). *Drug Metab. Rev.* **37**, 511–564.

Bricogne, G., Blanc, E., Brandl, M., Flensburg, C., Keller, P., Paciorek, W., Roversi, P., Sharff, A., Smart, O. S., Vonrhein, C. & Womack, T. O. (2011). *BUSTER* v.2.10.0. Global Phasing Ltd, Cambridge, England.

Brooke, E. W., Davies, S. G., Mulvaney, A. W., Pompeo, F., Sim, E. & Vickers, R. J. (2003). *Bioorg. Med. Chem.* **11**, 1227–1234.

Brown-Elliott, B. A. & Wallace, R. J. (2002). *Clin. Microbiol. Rev.* **15**, 716–746.

Case, D. A. *et al.* (2012). *AMBER* 12. University of California, San Francisco, USA.

Chen, V. B., Arendall, W. B., Headd, J. J., Keedy, D. A., Immormino, R. M., Kapral, G. J., Murray, L. W., Richardson, J. S. & Richardson, D. C. (2010). *Acta Cryst.* D**66**, 12–21.

Cocaign, A., Bui, L.-C., Silar, P., Chan Ho Tong, L., Busi, F., Lamouri, A., Mougin, C., Rodrigues-Lima, F., Dupret, J.-M. & Dairou, J. (2013). *Appl. Environ. Microbiol.* **79**, 4719–4726.

Deloménie, C., Fouix, S., Longuemaux, S., Brahimi, N., Bizet, C., Picard, B., Denamur, E. & Dupret, J.-M. (2001). *J. Bacteriol.* **183**, 3417–3427.

Emsley, P., Lohkamp, B., Scott, W. G. & Cowtan, K. (2010). *Acta Cryst.* D**66**, 486–501.

Flores, A. R., Parsons, L. M. & Pavelka, M. S. (2005). *Microbiology*, **151**, 521–532.

Fullam, E., Kawamura, A., Wilkinson, H., Abuhammad, A., Westwood, I. & Sim, E. (2009). *Protein J.* **28**, 281–293.

Fullam, E., Talbot, J., Abuhammed, A., Westwood, I., Davies, S. G., Russell, A. J. & Sim, E. (2013). *Bioorg. Med. Chem. Lett.* **23**, 2759–2764.

Fullam, E., Westwood, I. M., Anderton, M. C., Lowe, E. D., Sim, E. & Noble, M. E. M. (2008). *J. Mol. Biol.* **375**, 178–191.

Griffith, D. E., Girard, W. M. & Wallace, R. J. (1993). *Am. Rev. Respir. Dis.* **147**, 1271–1278.

Hanwell, M. D., Curtis, D. E., Lonie, D. C., Vandermeersch, T., Zurek, E. & Hutchison, G. R. (2012). *J. Cheminform.* **4**, 17.

Hein, D. W., McQueen, C. A., Grant, D. M., Goodfellow, G. H., Kadlubar, F. F. & Weber, W. W. (2000). *Drug Metab. Dispos.* **28**, 1425–1432.

Holton, S. J., Dairou, J., Sandy, J., Rodrigues-Lima, F., Dupret, J.-M., Noble, M. E. M. & Sim, E. (2005). *Acta Cryst.* F**61**, 14–16.

Jönsson, B. E., Gilljam, M., Lindblad, A., Ridell, M., Wold, A. E. & Welinder-Olsson, C. (2007). *J. Clin. Microbiol.* **45**, 1497–1504.

Kabsch, W. (2010). *Acta Cryst.* D**66**, 125–132.

Kubiak, X., Dairou, J., Dupret, J.-M. & Rodrigues-Lima, F. (2013). *Expert Opin. Drug Metab. Toxicol.* **9**, 349–362.

Kubiak, X., Dervins-Ravault, D., Pluvinage, B., Chaffotte, A. F., Gomez-Valero, L., Dairou, J., Busi, F., Dupret, J.-M., Buchrieser, C. & Rodrigues-Lima, F. (2012). *Biochem. J.* **445**, 219–228.

Kubiak, X., Li de la Sierra-Gallay, I., Chaffotte, A. F., Pluvinage, B., Weber, P., Haouz, A., Dupret, J.-M. & Rodrigues-Lima, F. (2013). *J. Biol. Chem.* **288**, 22493–22505.

Lambert, P. A. (2002). *J. Appl. Microbiol.* **92**, 46S–54S.

Laskowski, R. A., MacArthur, M. W., Moss, D. S. & Thornton, J. M. (1993). *J. Appl. Cryst.* **26**, 283–291.

Martins, M., Pluvinage, B., Li de la Sierra-Gallay, I., Barbault, F., Dairou, J., Dupret, J.-M. & Rodrigues-Lima, F. (2008). *J. Mol. Biol.* **383**, 549–560.

Morris, G. M., Huey, R., Lindstrom, W., Sanner, M. F., Belew, R. K., Goodsell, D. S. & Olson, A. J. (2009). *J. Comput. Chem.* **30**, 2785–2791.

Nash, K. A., Brown-Elliott, B. A. & Wallace, R. J. (2009). *Antimicrob. Agents Chemother.* **53**, 1367–1376.

Nessar, R., Cambau, E., Reyrat, J. M., Murray, A. & Gicquel, B. (2012). *J. Antimicrob. Chemother.* **67**, 810–818.

Payton, M., Auty, R., Delgoda, R., Everett, M. & Sim, E. (1999). *J. Bacteriol.* **181**, 1343–1347.

Payton, M., Gifford, C., Schartau, P., Hagemeier, C., Mushtaq, A., Lucas, S., Pinter, K. & Sim, E. (2001). *Microbiology*, **147**, 3295–3302.

Payton, M., Mushtaq, A., Yu, T.-W., Wu, L.-J., Sinclair, J. & Sim, E. (2001). *Microbiology*, **147**, 1137–1147.

Phillips, J. C., Braun, R., Wang, W., Gumbart, J., Tajkhorshid, E., Villa, E., Chipot, C., Skeel, R. D., Kalé, L. & Schulten, K. (2005). *J. Comput. Chem.* **26**, 1781–1802.
Pierre-Audigier, C., Ferroni, A., Sermet-Gaudelus, I., Le Bourgeois, M., Offredo, C., Vu-Thien, H., Fauroux, B., Mariani, P., Munck, A., Bingen, E., Guillemot, D., Quesne, G., Vincent, V., Berche, P. & Gaillard, J.-L. (2005). *J. Clin. Microbiol.* **43**, 3467–3470.
Pluvinage, B., Dairou, J., Possot, O. M., Martins, M., Fouet, A., Dupret, J.-M. & Rodrigues-Lima, F. (2007). *Biochemistry*, **46**, 7069–7078.
Pluvinage, B., Li de la Sierra-Gallay, I., Kubiak, X., Xu, X., Dairou, J., Dupret, J.-M. & Rodrigues-Lima, F. (2011). *FEBS Lett.* **585**, 3947–3952.
Ramirez, M. S. & Tolmasky, M. E. (2010). *Drug Resist. Updat.* **13**, 151–171.
Ripoll, F., Pasek, S., Schenowitz, C., Dossat, C., Barbe, V., Rottman, M., Macheras, E., Heym, B., Herrmann, J.-L., Daffé, M., Brosch, R., Risler, J.-L. & Gaillard, J.-L. (2009). *PLoS One*, **4**, e5660.
Rolfe, N. E., Garcia, C., Widen, R. H. & Taylor, S. P. (2013). *J. Med. Microbiol.* **62**, 1089–1091.
Rottman, M., Catherinot, E., Hochedez, P., Emile, J.-F., Casanova, J.-L., Gaillard, J.-L. & Soudais, C. (2007). *Infect. Immun.* **75**, 5898–5907.
Sandy, J., Holton, S., Fullam, E., Sim, E. & Noble, M. (2005). *Protein Sci.* **14**, 775–782.
Santarsiero, B. D., Yegian, D. T., Lee, C. C., Spraggon, G., Gu, J., Scheibe, D., Uber, D. C., Cornell, E. W., Nordmeyer, R. A., Kolbe, W. F., Jin, J., Jones, A. L., Jaklevic, J. M., Schultz, P. G. & Stevens, R. C. (2002). *J. Appl. Cryst.* **35**, 278–281.
Sikora, A. L., Frankel, B. A. & Blanchard, J. S. (2008). *Biochemistry*, **47**, 10781–10789.
Sim, E., Abuhammad, A. & Ryan, A. (2014). *Br. J. Pharmacol.* **171**, 2705–2725.
Sim, E., Fakis, G., Laurieri, N. & Boukouvala, S. (2012). *Adv. Pharmacol.* **63**, 169–205.
Sim, E., Sandy, J., Evangelopoulos, D., Fullam, E., Bhakta, S., Westwood, I., Krylova, A., Lack, N. & Noble, M. (2008). *Curr. Drug Metab.* **9**, 510–519.
Sim, E., Walters, K. & Boukouvala, S. (2008). *Drug Metab. Rev.* **40**, 479–510.
Sohn, H., Lee, K.-S., Ko, Y.-K., Ryu, J.-W., Woo, J.-C., Koo, D.-W., Shin, S.-J., Ahn, S.-J., Shin, A.-R., Song, C.-H., Jo, E.-K., Park, J.-K. & Kim, H.-J. (2008). *Int. J. Antimicrob. Agents*, **31**, 567–571.
Soroka, D., Dubée, V., Soulier-Escrihuela, O., Cuinet, G., Hugonnet, J.-E., Gutmann, L., Mainardi, J.-L. & Arthur, M. (2014). *J. Antimicrob. Chemother.* **69**, 691–696.
Tamura, K., Peterson, D., Peterson, N., Stecher, G., Nei, M. & Kumar, S. (2011). *Mol. Biol. Evol.* **28**, 2731–2739.
Tortoli, E. (2003). *Clin. Microbiol. Rev.* **16**, 319–354.
Weber, W. W. & Cohen, S. N. (1967). *Mol. Pharmacol.* **3**, 266–273.
Westwood, I. M., Bhakta, S., Russell, A. J., Fullam, E., Anderton, M. C., Kawamura, A., Mulvaney, A. W., Vickers, R. J., Bhowruth, V., Besra, G. S., Lalvani, A., Davies, S. G. & Sim, E. (2010). *Protein Cell.*, **1**, 82–95.
Winn, M. D. *et al.* (2011). *Acta Cryst.* D**67**, 235–242.